Published in final edited form as:
Neurotoxicology. 2013 July ; 0: 74–84. doi:10.1016/j.neuro.2013.04.004.

A Comparative Study of Protein Carbonylation and Mitochondrial Dysfunction Using the Neurotoxicants 1,3-Dinitrobenzene, 3-Nitropropionic Acid, and 3-Chloropropanediol

Stephen R. Steiner, **Evan Milton**, and **Martin A. Philbert**
Toxicology Program, Department of Environmental Health Sciences, School of Public Health, University of Michigan, Ann Arbor, MI, 48109-2029

Stephen R. Steiner: srs2sa@virginia.edu; Evan Milton: ecmilton@gmail.com; Martin A. Philbert: philbert@umich.edu

1. Introduction

The chemical intermediate 1,3-dinitrobenzene (1,3-DNB) serves as a model toxicant for acute energy deprivation syndromes that affect the central nervous system and lead to the development of clinical symptoms dependent on the exposure amount and duration (Cody et al., 1981; Philbert et al., 2000). Exposure to 1, 3-DNB causes symmetrical, bilateral gliovascular lesions distinctive of the brainstem regions affected in other chemical-induced mitochondrial encephalopathies, Leigh's syndrome, and Wernicke's encephalopathy (Philbert et al., 1987). The primary cellular target in the initial phase of 1,3-DNB intoxication are type 1 astrocytes found within the affected brainstem nuclei (Philbert et al., 1987; Romero et al., 1996). Although the molecular mechanism that underlies the selective nature of 1,3-DNB neurotoxicity is still undetermined, research findings support a mechanism that includes, but is not limited to, metabolic perturbation through the inhibition of pyruvate dehydrogenase and adenosine deaminase that could contribute to increased reactive oxygen species (ROS) production, loss of the mitochondrial membrane potential ($\Delta\Psi_m$) and induction of the mitochondrial permeability transition (MPT) (Romero et al., 1995; Tjalkens et al., 2000; Miller et al., 2011; Wang et al., 2012). 1,3-DNB-induced oxidative stress and mitochondrial dysfunction has also been linked to the oxidative carbonylation of specific proteins distributed within different intracellular locations (Steiner and Philbert 2011). Overall, these findings suggest that oxidative stress and altered enzyme function, meditated through structural alteration, early in 1,3-DNB neurotoxicity may be indicative of downstream metabolic derangement and the development of cellular dysfunction.

The accumulation of proteins damaged by oxidative carbonylation is an established hallmark of pathology observed within the nervous system, the detection of which has been routinely used as an indication of increased oxidative stress within the cellular environment (Smith et al.,1998; Aksenov et al., 2001; Castegna et al., 2002; Choi et al., 2003; Madian and Regnier 2011). Oxidative carbonylation alters protein structure and function through the irreversible, selective modification of specific amino acid residues (Dalle-Donne et al., 2006; Nyström

Correspondence to: Martin A. Philbert, philbert@umich.edu.
Present Address: 1800 Jefferson Park Avenue, Charlottesville, VA 22903
Present Address: 1822 SPH I, 1415 Washington Heights, Ann Arbor, MI 48109

2005). Oxidative stress overwhelms cellular mechanisms of ROS scavenging which increases the likelihood that susceptible proteins become structurally damaged by oxidative carbonylation. Another factor that determines protein susceptibility to carbonylation is the intracellular localization of a specific protein. Proteins located in close proximity to ROS-generating mechanisms, such as the mitochondrial protein complexes that mediate aerobic respiration, are prone to oxidative damage when metabolic disturbances lead to increased mitochondrial ROS production (Gibson 2005; Sas et al., 2007). 1,3-DNB exposure stimulates increased superoxide anion production that occurs prior to functional loss of the $\Delta\Psi_m$ (Steiner and Philbert 2011). This study demonstrated that exposure to 1,3-DNB resulted in the oxidative carbonylation of specific protein targets prior to the development of cellular manifestations of toxicity. The array of proteins oxidized during exposure to 1,3-DNB demonstrate how neurotoxicity may develop through a pathway that includes, but is not solely limited to, oxidation of mitochondrial proteins.

The purpose of the current study is to determine whether the pattern of 1,3-DNB-induced protein carbonylation is unique to the mechanism of1,3-DNB neurotoxicity. This study was designed as a comparative analysis using other neurotoxicants that disrupt energy production through mechanisms that involve oxidative stress. Identifying whether protein carbonylation exists in other chemical-induced mechanisms of cellular toxicity may help elucidate 1) specific targets of protein carbonylation that drive the development of 1,3-DNB neurotoxicity or 2) if protein carbonylation exists as a nonspecific outcome related to increased ROS production. The other neurotoxicants included in this study are 3-chloropropanediol (3-CPD) and 3-nitropropionic acid (3-NPA). 3-CPD is a metabolite of α-chlorohydrin and has been used as a model of chemical-induced energy deprivation syndromes (Cavanagh and Nolan 1993; Willis et al., 2004; Brown et al., 2011). 3-CPD targets Type 1 brainstem astrocytes and likely disrupts cellular function through alterations in redox state that promote increased oxidative stress (Skamarauskas et al., 2007). 3-NPA disrupts mitochondrial function through the suicide inhibition of succinate dehydogenase and increased formation of ROS, in addition to promoting the formation of protein carbonylation *in vivo* (La Fontaine et al., 2000; Phelka et al., 2003; Huang et al., 2006; Sandhir et al., 2010).

We identified and implemented the use of subtoxic concentrations of each chemical that did not induce significant reductions in cellular viability, but would result in perturbations of mitochondrial function. By using subtoxic concentrations of each toxicant, our goal was to increase the likelihood of successfully identifying specific molecular targets of oxidative carbonylation that could potentially be masked during the onset of terminal pathological mechanisms that incorporate substantial increases in oxidative stress, leading to widespread protein oxidation (Bizzozero et al., 2006; Dasgupta et al., 2012). Identifying the ideal subtoxic concentrations for use in this study was performed by conducting concentration-dependent analyses over a 48 hour exposure period using a MTS-based cellular viability assay. Analysis of mitochondrial function was performed using the fluorescent probe, TMRM. 2D PAGE followed by immunodetection was used to detect protein carbonylation in response to toxicant exposure. Carbonylated proteins were then identified using tandem mass spectrometry. The results of this study demonstrated that exposure to subtoxic concentrations of 1,3-DNB, 3-CPD, and 3-NPA toxicant resulted not only in concentration-dependent mitochondrial dysfunction, but also identified patterns of protein carbonylation that contained targets of oxidative carbonylation conserved among each treatment group along with specific proteins identified only within certain treatment groups.

2. Materials and Methods

2.1. Chemicals

Cell culture media and additional cell culture materials were obtained from Gibco (Invitrogen, Carlsbad, CA). The CellTiter 96 MTS assay was obtained from Promega (Madison, WI). The flurorescent probe, TMRM, was obtained from Molecular Probes (Invitrogen Eugene, OR). Oxyblot immunodetection materials were obtained from Chemicon (Millipore, Billerica, MA). Secondary antibodies, 2D Clean-Up kits, and Destreak rehydration buffer were obtained from GE Healthcare (Piscataway, NJ). IPG Readystrips and 12% Tris-HCl Readygels were obtained from Bio-Rad (Hercules, CA). The BCA protein quantification reagents were obtained from Pierce (Thermo Scientific, Rockford, IL). PVDF membranes used for immunoblotting were obtained from Millipore (Billerica, MA). All remaining reagents were of analytical grade and were obtained from Sigma-Aldrich (St. Louis, MO).

2.2. Cell Culture

DI TNC1 cells were obtained from the American Type Culture Collection (ATCC). The DI TNC1 cell line was established from cultured, type 1 astrocytes originating from 1-day old rat brain diencephalon tissue (Radany EH et al., 1992). Cells were maintained in a humidified incubator at 37°C in an atmosphere of 5% CO_2. DMEM containing 4.5 g/L D-glucose, L-glutamine, 10% fetal bovine serum, and 1% penicillin-streptomycin-glutamine mixture was the media used for maintenance of cell growth. Cell culture passages 5 through 25 were used for all experiments.

2.3. MTS assay

The CellTiter 96 cell proliferation assay was used to measure concentration-dependent deficits in metabolic activity of DI TNC1 cells exposed to concentrations of 1,3-DNB, 3-NPA, and 3-CPD within a 48-hour time period. The CellTiter 96 quantifies cellular proliferation, via colorimetric measurement, using a solution that contains a tetrazolium salt which is converted into formazan by cellular dehydrogenases within viable cells. DI TNC1 cells were cultured at a density of approximately 5000 cells/well in a 96-well tissue culture plate. Cultures were allowed to proliferate for 48 hrs, without reaching full confluence, before addition of 1 μM, 10 μM, 100 μM, 500 μM, and 1 mM concentrations of 1,3-DNB, 3-NPA, and 3-CPD in DMEM containing 10% FBS and 1% PSG. After each 48 hr exposure period, the media from each well was replaced with equivalent volumes of serum-free, phenol-free DMEM containing 20 μL MTS/PMS solution/ well. After 1.5 hr of incubation, formazan production was measured at an absorbance of 490 nm in a Gemini SpectraMax spectrophotometer (Molecular Devices, Sunnyvale, CA). The mean absorbance measurements from four independent experiments per exposure group were graphed as percentages ± SEM of the DMSO (v/v) control.

2.4. Laser Scanning Confocal Microscopy

Confocal microscopy was used to study the effect exposure to either 1,3-DNB, 3-NPA, and 3-CPD had on DI NTC1 mitochondrial function. DI TNC1 cells were grown on 22 mm round, glass coverslips and treated with 1 μM, 10 μM, and 100 μM concentration of each chemical for 48 hrs, using DMSO (%0.05 v/v) as a vehicle control. Subsequent to each exposure period, $\Delta\Psi_m$ was measured by incubating the cells in 20 mM HBSS/HEPES buffer containing 500 nM TMRM for 15 min at 37°C. To determine whether limiting oxidative stress could prevent loss of $\Delta\Psi_m$, DI TNC1 cells were pretreated with 600 μM deferoxamine for 20 minutes before incubation with each toxicant. After individual groups of treated cells were incubated in buffer solution containing TMRM, the coverslips were

placed in a heated stage for live-cell imaging analysis. Confocal analysis was conducted using an Olympus Fluoview/FV300 in combination with an inverted Olympus IX-70 microscope. The confocal microscope was fitted with an arrangement of Argon and HeNe lasers (Melles Griot) with parameters for the TMRM probe set for excitation at 543 nm and peak emission at 576 nm. Images were captured using a 60x oil immersion lens at an exposure rate of 2.41s/scan in order to limit photobleaching of the dyes. Approximately 2% of the maximum laser intensity was used for analyzing TMRM fluorescence. Mean fluorescence intensities from three independent experiments, ~ 8–10 cells per experiment, were measured using Adobe Photoshop and graphed using Microsoft Excel.

2.5. Protein Sample Preparation

DI TNC1 cells were grown to <90% confluence in 75 cm^2 flasks and exposed to 100 μM concentrations of 1,3-DNB, 3-NPA, and 3-CPD for 48 hrs. After exposure, protein samples were isolated from each exposure group using a protocol based upon the MITOISO1 isolation kit (Sigma-Aldrich). Oxyblot analysis was conducted using three separate biological replicates per treatment group, consisting of protein isolated from pooled cells derived from 6–7 flasks/treatment. Cells were homogenized using a teflon tissue grinder and glass pestle in 10 volumes of extraction buffer that contained 2 mg/ml bovine serum albumin. The extraction buffer used was composed of 220 mM mannitol, 70 mM sucrose, 0.5 mM EGTA, and 2 mM HEPES at a final pH of 7.4. The homogenate was transferred to a 15 ml conical tube and centrifuged at 500 × g for 5 minutes. The supernatant was then removed, centrifuged at 11000 × g, and the pellet resuspended in extraction buffer. Resuspension in extraction buffer occurred two more times so as to thoroughly wash the pellet. Once the protein pellet was resuspended in storage buffer containing 10 mM, HEPES, 250 mM sucrose, 1 mM ATP, 0.08 mM ADP, 5 mM sodium succinate, 2 mM K_2HPO_4, and 1mM DTT, a protease inhibitor cocktail was added to each sample before protein concentrations were quantified using the BCA Protein Assay kit. Fresh protein samples were used for each experiment presented in this study. The remaining protein samples were placed in storage at −80°C.

2.6. Two-dimensional (2D) gel electrophoresis

Aliquots of sample containing approximately 70 μg of protein were prepared for both SYPRO ruby staining and detection of protein carbonyls through Oxyblot analysis. Protein samples designated for Oxyblot analysis were derivatized for approximately 15 minutes at room temperature in a 1x dinitrophenylhydrazine (DNPH) solution freshly prepared each time from a stock solution provided for in each Oxyblot immunodetection kit. This reaction occurs when the carbonyl groups found on protein side chains react with DNPH form 2,4-dinitrophenylhydrazone, the chemical derivative that is detected using subsequent immunoblot analysis. Excess salts and other impurities were removed from each set of samples using a 2-D Clean-Up kit. Protein precipitates were incubated in wash buffer for approximately an hour prior to centrifugation at 12,000 × g for 5 min. Once the wash buffer was removed, 200 μl Destreak rehydration buffer containing 2.5 μL/mL IPG buffer, pH 3–10, was added to the protein pellet. The pellet was centrifuged at 12,000 × g in order to remove residual insoluble material that might hinder isoelectric focusing. Each sample was then added to a ReadyStrip IPG Strip 7 cm, pH 3–10. The IPG gel strips were actively rehydrated, overnight, in the IEF focusing tray of the Protean IEF cell at an electric current of 50 μA/IPG strip at a temperature of 20°C. Isoelectric focusing was performed, also overnight, using a voltage of 4000 V for a minimum of 20,000 Vh at 20°C. Prior to second dimension separation, the IPG strips were equilibrated for approximately 30 min in 0.375 m Tris-HCl (pH 8.8) buffer containing 6 M urea, 2% SDS, 20% glycerol, and 2% (w/v) dithiothreitol. The IPG strips were then placed on ReadyGels 12% Tris-HCl in Mini-Protean

III systems for electrophoresis. For the second dimension separation, the gels were run at a constant voltage of 100 V for approximately 1.45 h.

2.7. SYPRO Ruby staining

Gels were fixed in 50% methanol and 7% acetic acid twice, each for 30 min. Approximately 60 ml of SYPRO stain was added after the fixative was removed and the gels were stained overnight at room temperature. The gels were then washed in 10% methanol and 7% acetic acid and visualized in a Fujifilm FLA-5000 imaging system using Image Reader software.

2.8. Western Blot Analysis

2D gels designated for Oxyblot analysis were transferred to PVDF membranes. The PVDF membranes were exposed to blocking buffer for 45 min and subsequently incubated overnight at 4°C in rabbit primary antibody specific to 2,4-dinitrophenylhydrazone (1:150). After removal of the primary antibody, the membranes were then washed 4 times, using TBS-T each time for a total for 5 minutes/wash. Membranes were then incubated in TBS-T containing an anti-rabbit, alkaline phophatase-labeled secondary antibody (1:10000), used for ECF-based immunodetection for approximately 1 hour at room temperature. After incubating the membranes in buffer containing secondary antibody, the membranes were again washed for a period of at least 2 hours prior to visualization. Images of the membranes were captured using the Fujifilm FLA-5000 imaging system and Image Reader software.

2.9. Tandem Mass Spectrometry

LC/MS/MS analysis and protocol were provided by the Michigan Proteome Consortium (www.proteomeconsortium.org). Images of both the SYPRO Ruby stained 2D gels and 2D Oxyblots were overlaid on one another and carbonylated proteins were matched with protein spots from the 2D gels for excision followed by mass spectrometric analysis. Serum albumin (2 mg/ml) was added to the protein isolation in order to remove excess lipids from the isolate and act as a reference protein marker, in order to aid in spot matching which was performed manually with aid of our colleagues at the Michigan Proteome Consortium. Electrophoretically separated proteins contained within gel plugs excised from each gel using the MassPrep robot were digested with trypsin. Target peptides were extracted from the gel plugs with 30 μl of 2% acetonitrile 0.1% TFA. 5 μL of MALDI matrix was added to each extract and the extracts were dried using a Speed Vac. The peptides were dissolved in 5 μl of 60% ACN 0.1% TFA. An aliquot of each sample was spotted onto a MALDI target for MS/MS analysis. Protein identification was accomplished by our colleagues at the Michigan Proteome Consortium using the ProteinPilot search engine (Applied Biosystems), incorporating the use of the MASCOT search engine, along with the aid of the ProGroup algorithm and the International Protein Index (IPI) database. Each table contains identified protein is accompanied by an Unused ProtScore and a confidence value, expressed as a percentage, representing the confidence with which a peptide was identified. The Unused ProtScore is directly related to the confidence value of protein identification and is calculated using the number of identified peptide sequences that have not been assigned to other, higher scored proteins. The utility of this is that once a peptide spectrum has been used to support a particular protein's identification, that particular peptide spectrum can no longer be used to support the identification of any other proteins.

2.10. Statistical Analysis

MTS reduction data was expressed as mean ±SEM % DMSO control and compared using one-way ANOVA followed by a post-hoc Dunnett's test, with $p < 0.05$ representing significance difference between means. Confocal microscopy data was expressed as the mean of the observed fluorescence intensity ±SEM. Data from fluorescent images was also

compared using one-way ANOVA followed by a post-hoc Dunnett's test, with $p < 0.05$ representing a significant difference between the means. Statistical analysis was conducted using Graphpad Instat software (Version 3.05).

3. Results

3.1. Concentration-dependent analysis of metabolic activity in DI TNC1 cells exposed to 1,3-DNB, 3-NPA, and 3-CPD

Concentration-dependent metabolic activity in DI TNC1 cells exposed to each toxicant for 48 hours was analyzed according to MTS reduction (Figure 1). Cells exposed to 1,3-DNB for 48 hrs exhibited a concentration-dependent loss in metabolic activity, culminating at the 1 mM concentration (~48% DMSO control). Although a concentration-dependent trend was not observed, some loss in metabolic activity occurred in DI TNC1 cells exposed to 10 μM, 500 μM, and 1mM 3-NPA. The largest decrease in metabolic activity was observed in the 1mM 3-NPA treatment group (~78% DMSO control). However, the decreases in metabolic activity observed after exposure to each of these concentrations were not statistically significant. Cells exposed to 3-CPD for 48 hours exhibited no change in metabolic activity.

3.2. Concentration-dependent analysis of mitochondrial function in DI TNC1 cells exposed to 1,3-DNB, 3-NPA, and 3-CPD

Maintenance of the $\Delta\Psi_m$ in DI TNC1 cells exposed to 1,3-DNB, 3-NPA, and 3-CPD over 48 hour periods was assessed using the fluorescent dye, TMRM. In order to study concentration-based thresholds of mitochondrial dysfunction using subtoxic concentrations of each toxicant, the concentration of each toxicant used in this portion of the analysis represent values below the cutoff concentration required to induce statistically significant metabolic deficits and changes in cellular morphology (unpublished data) over an exposure period of 48 hours. The concentrations used during this portion of the study were 1 μM, 10 μM, and 100 μM of each neurotoxicant. Statistically significant, concentration-dependent loss of TMRM fluorescence occurred in all treatment groups during the 48 hr exposure period when compared to the DMSO control (Figure 2). Deferoxamine (600 μM) was used to determine if antioxidant pretreatment could protect cells against oxidative stress-induced mitochondrial dysfunction and was shown to protect against statistically significant loss of TMRM fluorescence in each treatment group, except cells treated with 100 μM of either toxicant and 10 μM of 1,3-DNB (Figure 3).

3.3. Immunodetection and tandem mass spectrometric detection of protein carbonyls in DI TNC1 cells exposed to 1,3-DNB, 3-NPA and 3-CPD

We previously demonstrated that exposure to 1,3-DNB resulted in the carbonylation of specific DI TNC1 proteins (Steiner and Philbert 2011). As was our approach in the previous study, 2D Oxyblot analysis followed by tandem mass spectrometry was the method used to identify targets of protein carbonylation in toxicant-treated DI TNC1 cells. The concentration selected for analysis of protein carbonylation was 100 μM of each toxicant since cells exposed to this particular concentration for 48 hours resulted in statistically significant perturbation of mitochondrial function without complete loss of the $\Delta\Psi_m$ and no significant disruption in metabolic capacity.

2D Oxyblot analysis revealed that specific proteins were sensitive to 100 μM 1,3-DNB, 100 μM 3-CPD, and 100 μM 3-NPA-induced carbonylation after 48 hours of exposure (Table 1, Table 2, Table 3, respectively). In addition, Oxyblot analysis for each treatment group revealed that not all proteins within a 2D gel exhibit anti-2,4-dinitrophenylhydrazone immunoreactivity, emphasizing the selective nature of protein carbonylation within each 1,3-DNB, 3-CPD, and 3-NPA treatment. The carbonylation patterns observed in each

treatment group were similar to each other with respect to the region of the gel within which each carbonylated proteins migrated. Most of the carbonylated proteins appeared within a PI range of approximately 4–7 and a mass range of 50–70 kDa. However, there were differences in the number of carbonylated proteins identified within each separate treatment. LC/MS/MS analysis revealed that calreticulin precursor, reticulocalbin-3, actin, and the serum albumin marker were carbonylated in the 1,3-DNB and 3-CPD treatment groups. Carbonylated proteins also identified in the 1,3-DNB exposure group included F1-ATP synthase beta-subunit and protein disulfide isomerase. Additional carbonylated proteins identified in the 3-NPA exposure group included Grp78 glucose-regulated protein, tumor rejection antigen gp96, 40S ribosomal protein SA, and a member of the pumilio-family RNA-binding proteins, D19Bwg1357e (Kuo et al., 2009).

4. Discussion

This study demonstrated how exposure to each of the three neurotoxicants tested led to the formation of specific carbonylated proteins in DI TNC1 cells. DI TNC1 cells exposed to 1,3-DNB and 3-NPA exhibited concentration- dependent decreases in metabolic activity over a 48-hour exposure period and cells exposed to subtoxic concentrations of each of the three toxicants for 48 hours induced concentration-dependent decreases in TMRM fluorescence, signifying partial loss of $\Delta\psi_m$. Pretreatment with the antioxidant, deferoxamine, provided some protection against loss of TMRM fluorescence in cells exposed to the lowest concentrations of each toxicant and in the treatment groups exposed to midrange (10 μM) concentrations of 3-NPA and 3-CPD. Exposure to 1,3-DNB, 3-NPA, and 3-CPD each resulted in a somewhat conserved pattern of protein carbonylation, suggesting that some proteins are inherently susceptible to oxidative carbonylation regardless of the oxidizing mechanism. However, additional proteins carbonylated during exposure to 1,3-DNB and 3-NPA suggest that downstream cellular toxicity may develop through alternative molecular pathways mediated by oxidative stress in situations involving specific toxic insults.

The MTS cellular viability assay granted us the means by which subtoxic concentrations of each toxicant could be identified and used in subsequent analyses of mitochondrial function and protein carbonylation. Unlike the concentration-dependent analyses of 1,3-DNB and 3-NPA, exposure to increasing concentrations of 3-CPD for 48-hours did not result in either statistically significant or non-significant loss of metabolic activity. This particular finding may be explained by the concentration of toxicant and model cell line used in this study. Skamarauskas et al., 2007 demonstrated that the regional susceptibility of astrocytes to 3-CPD intoxication is at least, in part, due to the bioactivation of 3-CPD to a reactive monoaldehyde occurring in vulnerable brainstem nuclei. This study demonstrated that proliferating astrocytes, of neocortical and brainstem origin, and differentiated brainstem astrocytes are the most sensitive to 3-CPD intoxication. One implication from this work is that the relative resistance to 3-CPD-induced toxicity demonstrated by DI TNC1 cells may result from a cell-specific lack of the necessary enzymatic capacity for bioactivating 3-CPD to its toxic monoaldehyde intermediate. In addition, the cell viability studies conducted by Skamarauskas et al., 2007 demonstrated that significant loss within susceptible astrocyte populations did not occur until cells were exposed to concentrations of 3-CPD that exceeded 1mM for greater than 24 hours. It is possible that although the 48 hr exposure period used in our analysis was an appropriate time point for inducing outright toxicity, the concentrations of 3-CPD implemented were likely not enough to induce outright loss of cellular viability. Of note, a burst of formazan production was observed in the treatment groups exposed to 100 μM 3-NPA. Considering this increase was not statistically significant, it represents a possible increase or no change in metabolic activity when compared to the vehicle control. This is, however, an anomalous finding since the 10 μM and 500 μM 3-NPA treatment

groups both demonstrated loss in metabolic activity. It is especially intriguing considering that 1 μM , 10 μM , and 100 μM of 3-NPA caused a concentration-dependent loss of $\Delta\psi_m$, as demonstrated by decreasing TMRM fluorescence in exposed DI TNC1 cells (Figure 2). Review of the data from each individual MTS trial at this particular 100 μM 3-NPA concentration revealed no obvious outliers that might have otherwise skewed the mean. Given that the observed decreases in MTS reduction upon exposure to 3-NPA at any concentration were not statistically significant, future MTS analysis will include more trials for each concentration in order to confirm whether a statistically significant concentration-dependent decrease in function exists at these concentrations and whether the burst of formazan production observed at 100 μM 3-NPA is truly an anomaly.

We observed that treatment with 1 μM, 10 μM, or 100 μM of either 1,3-DNB, 3-NPA, or 3-CPD over the course of 48 hours did not cause any significant reductions in cell viability. However, these concentrations were capable of inducing partial, yet statistically significant, loss of TMRM fluorescence in a concentration-dependent manner for each chemical tested during a 48 hr exposure period when compared to the vehicle control. Mitochondrial function can be disrupted at subtoxic concentrations of each neurotoxicant without affecting cell viability. This lends credence to the idea that constant exposure to low concentrations of these toxicants can ultimately result in cellular injury mediated through mechanisms that cause a breakdown in cellular energy by causing disruption of mitochondrial function. In order to determine whether oxidative stress contributed to loss of the $\Delta\Psi_m$, the antioxidant, deferoxamine, was administered to DI TNC1 cells prior to the addition of each toxicant. Pretreatment with deferoxamine prevented loss of TMRM fluorescence in almost all of the treatment groups except those in which the highest concentration of each toxicant was applied. These findings lend support to the conclusion that increased ROS production play a mechanistic role in the development of mitochondrial dysfunction upon exposure to each neurotoxicant. Additionally, it is likely that ROS production increases in concentration-dependent manner given that deferoxamine exerted its protective effect only when the smallest and midrange concentrations of each toxicant were used. Previous work from our lab demonstrated that a higher concentration (1 mM) of 1,3-DNB resulted in oxidative stress-mediated mitochondrial injury after only a few hours of exposure, in a time-dependent manner (Steiner and Philbert 2011). Coupled with the results from the present study, 1,3-DNB's deleterious effect on DI TNC1 mitochondria appear to be both concentration and time-dependent given that smaller concentions of 1,3-DNB also led to mitochondrial dysfunction, but that these effects were appreciated after 48 hours of exposure to 1,3-DNB rather than after only a few hours. An interesting finding within the current study is how exposure to subtoxic concentrations of1,3-DNB, 3-NPA, and 3-CPD all led to a similar concentration-dependent loss of the $\Delta\Psi_m$. What this may represent is that each manner of chemical-induced toxicity represented in this study may indirectly affect normal mitochondrial function through a mechanism that involves enhanced ROS production, even though distinct mechanisms of toxic action cannot be ruled out.

Certain proteins were identified as common targets of oxidative carbonylation within each group of cells exposed to either 1,3-DNB, 3-CPD, or 3-NPA. Calreticulin, reticulocalbin-3, actin, and serum albumin were the only carbonylated proteins identified within the 3-CPD treatment group. In addition to the aforementioned proteins, the F1-ATP synthase beta-subunit and protein disulfide isomerase were carbonylated after exposure to 1,3-DNB and 3-NPA. Exposure to 3-NPA also resulted in the carbonylation of Grp78, tumor rejection antigen gp 96, and D19Bwg1357e. The results presented in this study are the first to offer a comparison between the 1,3-DNB-induced pattern of oxidative carbonylation with patterns of oxidative carbonylation resultant from exposure to other neurotoxicants. Several of the proteins identified were previously identified as targets of oxidative carbonylation resulting from oxidative damage associated with various forms of neuropathology including

Alzheimer's disease, age-associated oxidation, and experimental autoimmune encephalomyelitis (Bizzozero et al., Choi et al., 2003; 2008; Prokai et al., 2007; Rabek et al., 2003; Smerjac et al., 2008; Temple et al., 2006). In addition, all of the carbonylated proteins, with the exception of D19Bwg1357e, reticulocalbin-3, and the 40S ribosomal protein SA, were identified in a previous analysis of 1,3-DNB-induced protein carbonylation (Steiner and Philbert 2011). This group of proteins includes proteins that are integral to the ER stress response, cytoskeletal structure, and mitochondrial function. These results suggest that this particular collection of carbonylated proteins carry an inherent susceptibility to increased levels of oxidative stress, regardless of the toxic insult. Though this study was designed to address patterns of toxicant-induced protein oxidation, the next logical series of experiments should not only include determining the amount of ROS produced from exposure to each toxicant, but also the level of carbonylation that each toxicant induces on individual proteins so that protein carbonylation can be analyzed from a quantifiable standpoint rather than solely a qualitative one. Future studies designed to quantify toxicant-induced ROS production and protein-specific carbonylation levels may identify a relationship between specific toxicants that lead to more robust generation of ROS and greater levels of protein carbonylation.

That carbonylation of these rather small, yet select, groups of proteins suggestively implies how a shared pathway to cellular injury may involve a mechanism of non-specific damage mediated by increased levels of ROS. For example, one particular protein that was a focus of discussion in our previous study and was again identified in this study as a target of protein carbonylation is the F1-ATP synthase beta-chain subunit. Not only is the beta-subunit a known target of protein carbonylation, but this is the second time that our lab has been able to report how 1,3-DNB exposure leads to the oxidative carbonylation of this particular mitochondrial protein (Dihazi et al., 2005; Prokai et al., 2007; Je et al., 2008; Steiner and Philbert 2011). The F1-ATP synthase beta-subunit's susceptibility to oxidative modification is further enhanced in this study by appreciating how the beta-subunit was also identified as a target of 3-NPA-mediated protein carbonylation. The identification of the F1-ATP synthase beta-subunit as a common target of both 1,3-DNB and 3-NPA-induced protein carbonylation illustrates how a common pathway to cellular injury may be mediated by non-specific oxidative damage to select proteins. This finding is even more intriguing when one considers that the toxicity elicited by 3-NPA and 1,3-DNB are thought to be, at least in part, due to mitochondrial injury, whereas recent evidence has demonstrated that 3-CPD likely exerts its neurotoxic effect by disrupting redox status in susceptible cells by depleting glutathione reserves and inhibiting glutathione-*S*-transferase (Skamarauskas et al., 2007). A potential shared mechanism by which both 1,3-DNB and 3-NPA disrupt mitochondrial function is through the inhibition of succinate dehydrogenase. 3-NPA is a recognized inhibitor of succinate dehydrogenase that causes electron chain dysfunction, loss of $\Delta\Psi_m$, ROS production and protein carbonyl formation (Gould et al., 1985; Brouillet et al., 1998; La Fontaine et al., 2000; Sandhir et al., 2010). Phelka et al., 2003 demonstrated that exposure to 1,3-DNB also inhibited succinate dehydrogenase activity in cortical and brainstem mitochondria in a side-by-side comparison with 3-NPA.This does not, however, rule out the presence of other toxicant-specific molecular targets that are involved in the cascade of events that ultimately leads to cellular injury.

An observation to note is how exposure to each toxicant resulted in specific patterns of carbonylation that included some, but not all, of these previously identified proteins. Our previous study demonstrated that exposure to the vehicle control alone and negative control samples that lacked the proper epitope for primary antibody binding resulted in some background signal intensity (vehicle control) or a complete lack of carbonylation signal (negative control) (Steiner and Philbert 2011). This finding supports the assertion that any observed differences regarding the presence or absence of certain carbonylated proteins may

be due to the particular toxicant exposure itself. Another important consideration regarding the results of this study that was initially discussed in previous work is how relatively few proteins were identified as targets of oxidative carbonylation when compared to the overall number of proteins present in a DI TNC1 cell's proteome; an observation made apparent by simply comparing an immunoblot with its corresponding 2D gel. This consistent finding might be explained by one of multiple reasons that include how only the most oxidationsensitive proteins are carbonylated at the toxicant concentrations used, that carbonylation stimulates proteasomal degradation of oxidized proteins, or that protein carbonyl formation may be dependent on molecular weight given that the majority of the carbonylated proteins identified in the current study were distributed among a mass range of 50–70 kDa (Floor and Wetzel 1998; Ceccarini et al., 2007; Tengowski et al., 2007). A recent study surveying current methods of detecting carbonylated proteins using immunoblotting discussed how derivatizing proteins with DNPH after electrophoresis resulted in the detection of more carbonyl-modified proteins than if one were to derivatize proteins prior to electrophoresis (Linares et al., 2011). Though this alternative technique may enhance detection of carbonylated proteins, in situ derivatization within the gel may result in more background artifact that could muddle reproducibility between replicate gels. Still, given that all of our analyses up to this point have implemented derivatization of protein samples prior to electrophoresis, it might be worth exploring this method as an alternative immunoblotting technique in order to optimize detection sensitivity. In addition, future experiments will also incorporate the use of a fluorescent tracking dye, such as SYPRO Tangerine, in order to confirm the efficacy with which individual proteins were transferred from the 2-D gel to the PVDF membrane.

In summary, this study provides important new insight into how protein carbonylation may mediate the neurotoxicity of 1,3-DNB and other neurotoxicants that target mitochondrial function through oxidative stress. This report is the first to compare the macromolecular targets of oxidative carbonylation between 1,3-DNB-induced neurotoxitcity and other forms of chemical-induced neurotoxicity. These findings provide evidence supporting the notion that although different forms of chemical-induced neurotoxicity may share common molecular pathways that lead to similar pathology within the nervous system, such as alterations within the structure of key proteins, cellular toxicity is likely dictated by a collection of different molecular changes occurring within specific cellular subtypes. Future studies intent on testing how protein function is altered when the structures of these specific proteins are modified through carbonylation need to be designed in order to assess whether the oxidative modification of individual proteins, select group of proteins, or some other as of yet undetermined mechanism not related to oxidation-induced structural changes contribute to the mitochondrial dysfunction and cellular injury observed in chemical-induced models of energy deprivation.

Acknowledgments

The authors gratefully acknowledge the assistance of Jennifer Fernandez and the Michigan Proteomics Core for their technical support. This research was supported by grants from the NIEHS (NIH T32-ES07062) and NIH (RO1-ES08846).

References

Aksenov MY, Aksenova MV, Butterfield DA, Geddes JW, Markesbery WR. Protein oxidation in the brain in Alzheimer's disease. Neuroscience. 2001; 103:373–383. [PubMed: 11246152]

Bizzozero OA, Ziegler JL, De Jesus G, Bolognani F. Acute depletion of reduced glutathione causes extensive carbonylation of rat brain proteins. J Neurosci Res. 2006; 83:656–667. [PubMed: 16447283]

Brown AM, Skamarauskas J, Lister T, Madjd A, Ray DE. Differential susceptibility of astrocytic and neuronal function to 3-chloropropanediol in the rat inferior colliculus. J Neurochem. 2011; 116:996–1004. [PubMed: 21155803]

Brouillet E, Guyot MC, Mittoux V, Altairac S, Condé F, Palfi S, Hantraye P. Partial inhibition of brain succinate dehydrogenase by 3-nitropropionic acid is sufficient to initiate striatal degeneration in rat. J Neurochem. 1998; 70:794–805. [PubMed: 9453576]

Castegna A, Aksenov M, Aksenova M, Thongboonkerd V, Klein JB, Pierce WM, Booze R, Markesbery WR, Butterfield DA. Proteomic identification of oxidatively modified proteins in Alzheimer's disease brain Part I: Creatine kinase BB, glutamine synthase, and ubiquitin carboxy-terminal hydrolase L-1. Free Rad Biol Med. 2002; 33:562–571. [PubMed: 12160938]

Cavanagh JB, Nolan CC. The neurotoxicity of alpha-chlorohydrin in rats and mice: II. Lesion topography and factors in selective vulnerability in acute energy deprivation syndromes. Neuropathol Appl Neurobiol. 1993; 19:471–479. [PubMed: 8121541]

Ceccarini V, Gee J, Fioretti E, Amici M, Angeletti M, Eleuteri AM, Keller JN. Protein oxidation and cellular homeostasis: emphasis on metabolism. Biochem Biophys Acta. 2007; 1773:93–104. [PubMed: 17023064]

Choi J, Malakowsky CA, Talent JM, Conrad CC, Carroll CA, Weintraub ST, Gracy RW. Anti-apoptotic proteins are oxidized by $A\beta_{25–35}$ in Alzheimer's fibroblasts. Biochim Biophys Acta. 2003; 1637:135–141. [PubMed: 12633901]

Cody TE, Witherup S, Hastings L, Stemmer K, Christian RT. 1,3-Dinitrobenzene: toxic effects in vivo and in vitro. J Toxicol Environ Health. 1981; 7:829–847. [PubMed: 7265311]

Dalle-Donne I, Aldini G, Carini M, Colombo R, Rossi R, Milzani A. Protein carbonylation, cellular dysfunction, and disease progression. J Cell Mol Med. 2006; 10:389–406. [PubMed: 16796807]

Dasgupta A, Zheng J, Bizzozero OA. Protein carbonylation and aggregation precede neuronal apoptosis induced by partial glutathione depletion. ASN NEURO. 2012; 4:161–174.

Dihazi H, Asif AR, Agarwal NK, Doncheva Y, Müller GA. Proteomic analysis of cellular response to osmotic stress in thick ascending limb of Henle's loop (TALH) cells. Mol Cell Proteomics. 2005; 4:1445–1458. [PubMed: 15975915]

Floor E, Wetzel MG. Increased protein oxidation in human substantia nigra pars compacta in comparison with basal ganglia and prefrontal cortex measured with an improved dinitrophenylhydrazine assay. J Neurochem. 1998; 70:268–275. [PubMed: 9422371]

Gibson BW. The human mitochondrial proteome: oxidative stress, protein modifications and oxidative phosphorylation. Int J Biochem Cell Biol. 2005; 37:927–934. [PubMed: 15743667]

Gould DH, Wilson MP, Hamar DW. Brain enzyme and clinical alterations induced in rats and mice by nitroaliphatic toxicants. Toxicol Lett. 1985; 27(1–3):83–89. [PubMed: 4060188]

Huang L, Sun G, Cobessi D, Wang AC, Shen JT, Tung EY, Anderson VE, Berry EA. 3-nitropropionic acid is a suicide inhibitor of mitochondrial respiration that, upon oxidation by complex II, forms a covalent adduct with a catalytic base arginine in the active site of the enzyme. J Biol Chem. 2006; 281:5965–5972. [PubMed: 16371358]

Je JH, Lee TH, Kim DH, Cho YH, Lee JH, Kim SC, Lee SK, Lee J, Lee MG. Mitochondrial ATP synthase is a target for TNBS-induced protein carbonylation in XS-106 dendritic cells. Proteomics. 2008; 8:2384–2393. [PubMed: 18563732]

Kuo MW, Wang SH, Chang JC, Chang CH, Huang LJ, Lin HH, Yu ALT, Li WH, Yu J. A novel puf-A gene predicted from evolutionary analysis is involved in the development of eyes and primordial germ-cells. PLOS ONE. 2009; 4(3):1–12.

La Fontaine MA, Geddes JW, Banks A, Butterfield DA. 3- nitropropionic acid induced in vivo protein oxidation in striatal and cortical synaptosomes: insights into Huntington's disease. Brain Res. 2000; 858:356–362. [PubMed: 10708687]

Linares M, Marín-García P, Méndez D, Puyet A, Diez A, Bautista JM. Proteomic approaches to identifying carbonylated proteins in brain tissue. J Proteome Res. 2011; 10:1719–1727. [PubMed: 21235272]

Madian AG, Regnier FE. Proteomic identification of carbonylated proteins and their oxidation sites. J Proteome Res. 2011; 9:3766–3780. [PubMed: 20521848]

Miller JA, Runkle SA, Tjalkens RB, Philbert MA. 1,3-dinitrobenzene-induced metabolic impairment through inactivation of the pyruvate dehydrogenase complex. Toxicol Sci. 2011; 122:502–511. [PubMed: 21551353]

Nyström T. Role of oxidative carbonylation in protein quality control and senescence. Embo J. 2005; 24:1311–1317. [PubMed: 15775985]

Phelka AD, Beck MJ, Philbert MA. 1,3-dinitrobenzene inhibits mitochondrial complex II in rat and mouse brainstem and cortical astrocytes. Neurotoxicology. 2003; 24:403–415. [PubMed: 12782105]

Philbert MA, Nolan CC, Cremer JE, Tucker D, Brown AW. 1,3-dinitrobenzene-induced encephalopathy in rats. Neuropathol Appl Neurobiol. 1987; 13:371–389. [PubMed: 3683748]

Philbert MA, Billingsley ML, Reuhl K. Mechanisms of injury in the central nervous system. Toxicol Pathol. 2000; 28:43–53. [PubMed: 10668990]

Prokai L, Yan L-J, Vera-Serrano JL, Stevens SM Jr, Forster MJ. Mass spectrometrybased survey of age-associated protein carbonylation in rat brain mitochondria. J Mass Spectrom. 2007; 42:1583–1589. [PubMed: 18085547]

Rabek JP, Boylston III WH, Papaconstantinou J. Carbonylation of ER chaperone proteins in aged mouse liver. Biochem Biophys Res Com. 2003; 305:566–572. [PubMed: 12763031]

Radany EH, Brenner M, Besnard F, Bigornia V, Bishop JM, Deschepper CF. Directed establishment of rat brain cell lines with the phenotypic characteristics of type 1 astrocytes. Proc Natl Acad Sci USA. 1992; 89:6467–71. [PubMed: 1378628]

Romero IA, Lister T, Richards HK, Seville MP, Wylie SP, Ray DE. Early metabolic changes during m-dinitrobenzene neurotoxicity and the possible role of oxidative stress. Free Radic Biol Med. 1995; 18:311–319. [PubMed: 7744316]

Romero IA, Ray DE, Chan MWK, Abbott NJ. An in vitro study of m-dinitrobenzene toxicity on the cellular components of the blood-brain barrier, astrocytes and endothelial cells. Toxicol Appl Pharmacol. 1996; 139:94–101. [PubMed: 8685913]

Sandhir R, Mehrotra A, Kamboj SS. Lycopene prevents 3-nitroproprionic acid-induced mitochondrial oxidative stress and dysfunctions in nervous system. Neurochem Int. 2010; 57:579–587. [PubMed: 20643176]

Sas K, Robotka H, Toldi J, Vécsei L. Mitochondria, metabolic disturbances, oxidative stress and the kynurenine system, with focus on neurodegenerative disorders. J Neurol Sci. 2007; 257:221–239. [PubMed: 17462670]

Skamarauskas J, Carter W, Fowler M, Madjd A, Lister T, Mavroudis G, Ray DE. The selective neurotoxicity produced by 3-chloropropanediol in the rat is not a result of energy deprivation. Toxicology. 2007; 232:268–276. [PubMed: 17321661]

Smerjac SM, Bizzozero OA. Cytoskeletal protein carbonylation and degradation in experimental autoimmune encephalomyelitis. J Neurochem. 2008; 105:763–772. [PubMed: 18088377]

Smith MA, Sayre LM, Anderson VE, Harris PLR, Beal MF, Kowall N, Perry G. Cytochemical demonstration of oxidative damage in Alzheimer disease by immunochemical enhancement of the carbonyl reaction with 2,4-Dinitrophenylhydrazine. J Histochem Cytochem. 1998; 46:731–735. [PubMed: 9603784]

Steiner SR, Philbert MA. Proteomic identification of carbonylated proteins in 1,3-dinitrobenzene neurotoxicity. Neurotoxicology. 2011; 32:362–373. [PubMed: 21402099]

Temple A, Yen T, Gronert S. Identification of specific protein carbonylation sites in model oxidations of human serum albumin. J Am Soc Mass Spectrom. 2006; 17:1172–1180. [PubMed: 16750385]

Tengowski MW, Feng D, Sutovsky M, Sutovsky P. Differential expression of genes encoding constitutive and inducible 20S proteasomal core subunits in the testis and epididymis of theophylline- or 1,3-dinitrobenzene-exposed rats. Biol Reprod. 2007; 76:149–163. [PubMed: 16988215]

Tjalkens RB, Ewing MM, Philbert MA. Differential cellular regulation of the mitochondrial permeability transition in an in vitro model of 1,3-dinitrobenzene-induced encephalopathy. Brain Res. 2000; 874:165–177. [PubMed: 10960601]

Wang Y, Liu X, Schneider B, Zverina EA, Russ K, Wijeyesakere SJ, Fierke CA, Richardson RJ, Philbert MA. Mixed inhibition of adenosine deaminase activity by 1,3-dinitrobenzene: a model for

understanding cell-selective neurotoxicity in chemically-induced energy deprivation syndromes in brain. Toxicol Sci. 2012; 125:509–521. [PubMed: 22106038]

Willis CL, Nolan CC, Reith SN, Lister T, Prior MJW, Guerin CJ, Mavroudis G, Ray DE. Focal astrocyte loss is followed by microvascular damage, with subsequent repair of the blood-brain barrier in the apparent absence of direct astrocyte contact. Glia. 2004; 45:325–337. [PubMed: 14966864]

- Subtoxic concentrations caused mitochondrial dysfunction without affecting viability
- Each neurotoxicant led to concentration-dependent decreases in TMRM fluorescence
- The antioxidant, deferoxamine, protected against loss of TMRM fluorescence
- Exposure to 100μM of each toxicant led to similar patterns of protein carbonylation

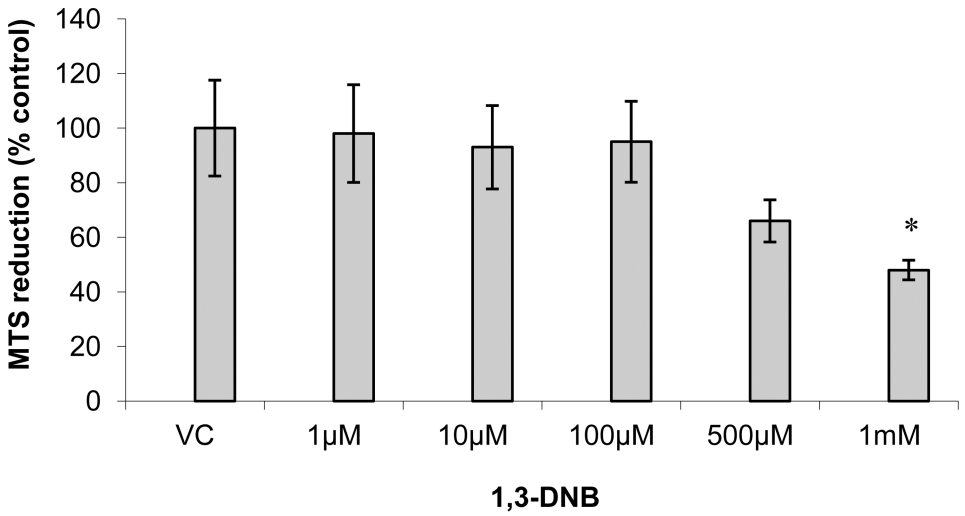

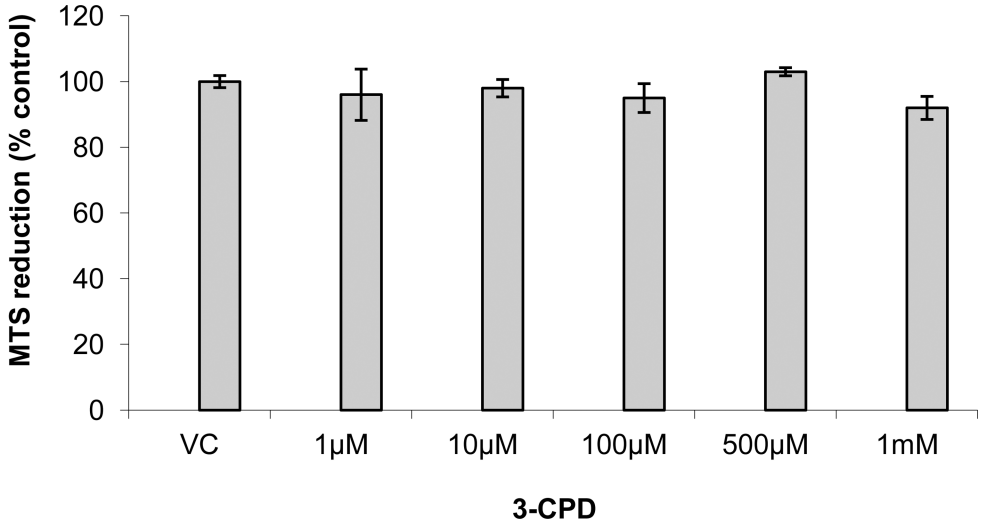

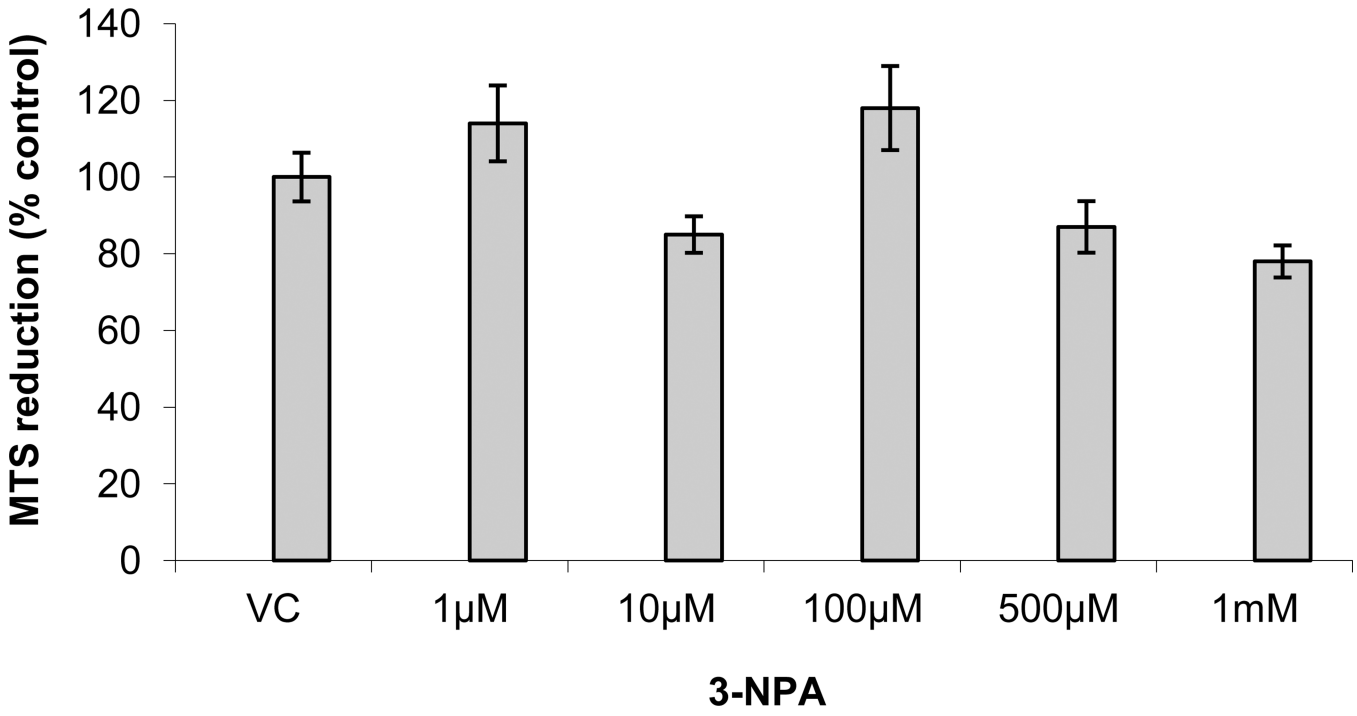

Figure 1.
Concentration-dependent decrease in MTS reductive capability of DI TNC1 cells exposed to 1,3-DNB, 3-CPD, and 3-NPA over a 48 hr period. Data is expressed as % DMSO control ± SEM (n=4) with statistical significance (*) if $p < 0.05$.

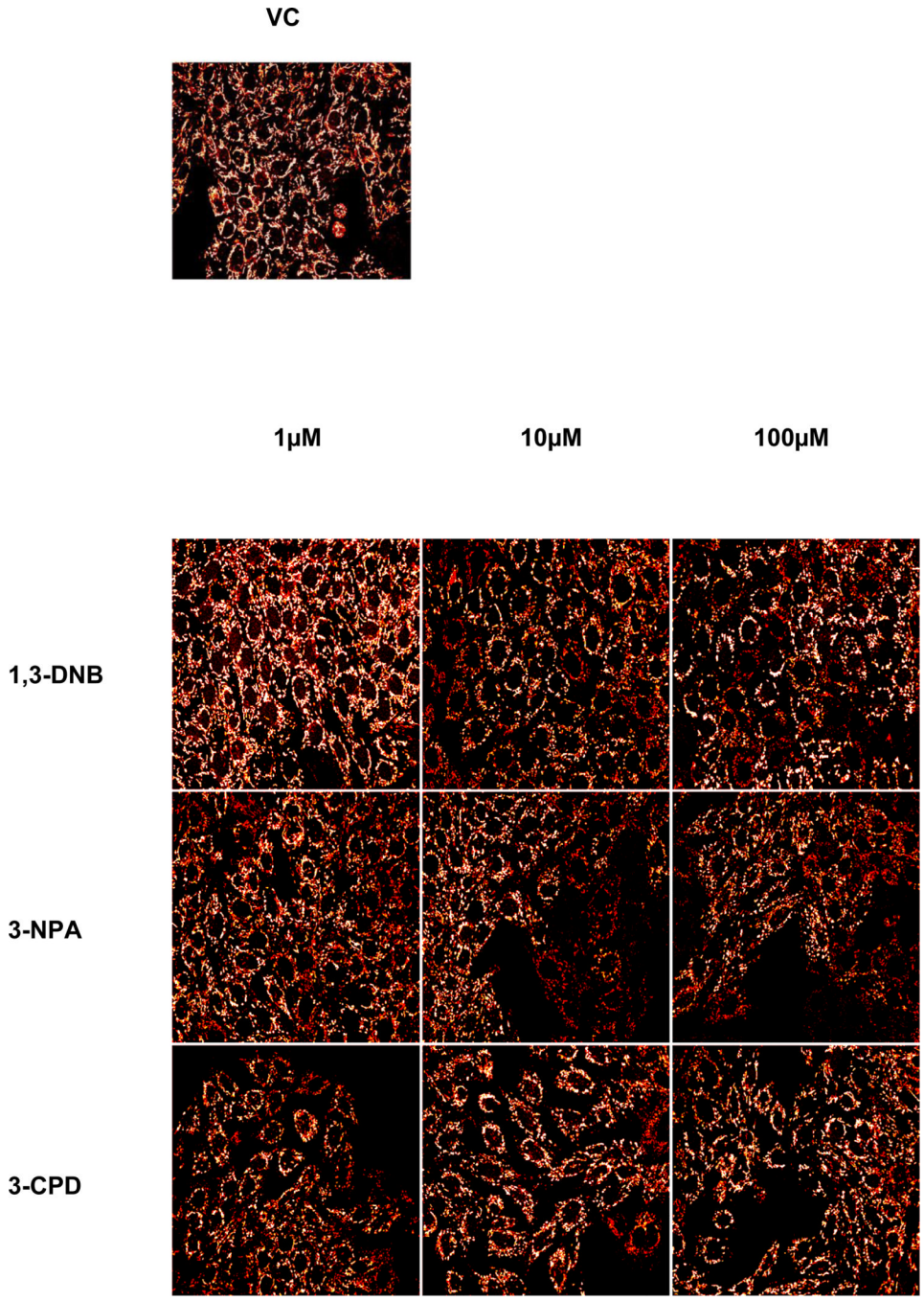

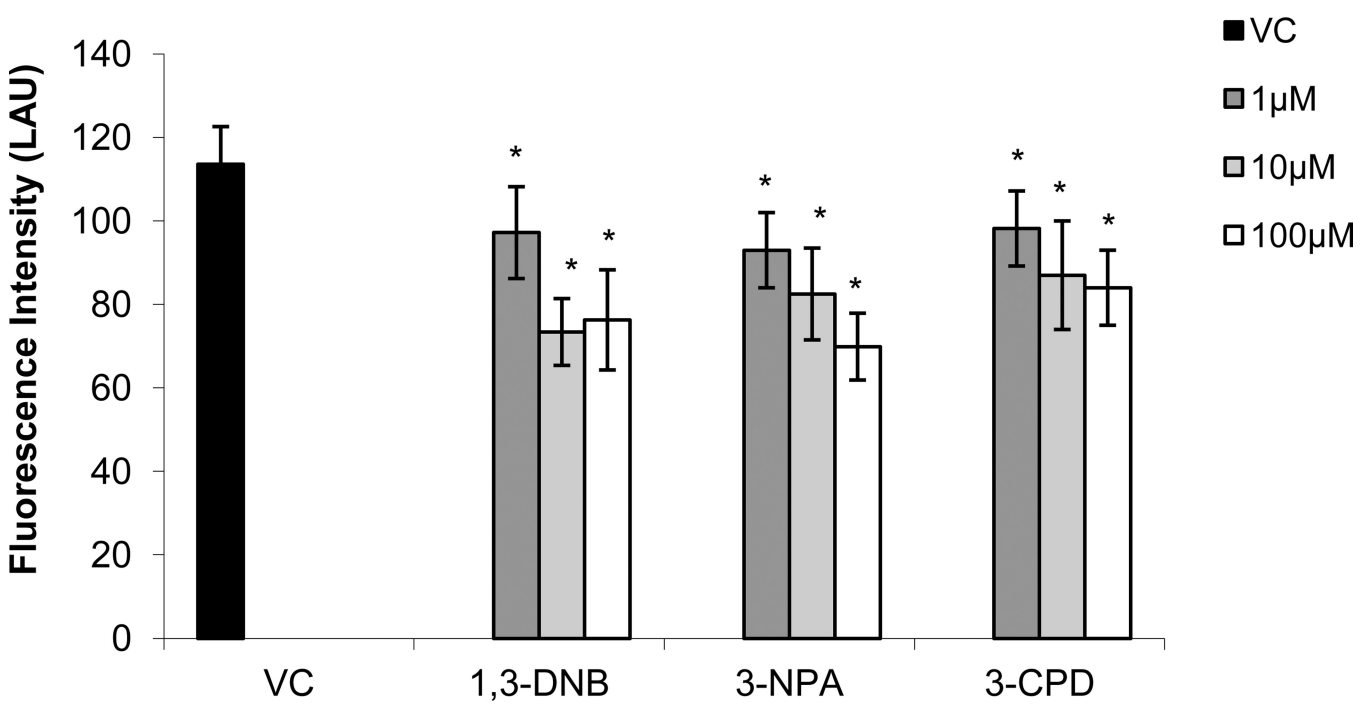

Figure 2.

Concentration-dependent loss of $\Delta\Psi_m$ in DI TNC1 cells measured over a 48 hr period using confocal microscopy. DI TNC1 cells were loaded with TMRM for 15 minutes after exposure to DMSO vehicle control and 1 μM, 10 μM, or 100 μM concentrations of 1,3-DNB, 3-NPA, or 3-CPD. Changes in TMRM fluorescence after a 48 hr exposure to each toxicant were measured and graphed as linear arbitrary units (LAU) in three independent experiments (8–10 cells per experiment). Values are expressed as mean ± SEM with statistical significance if $p < 0.05$ when compared to DMSO vehicle control (*).

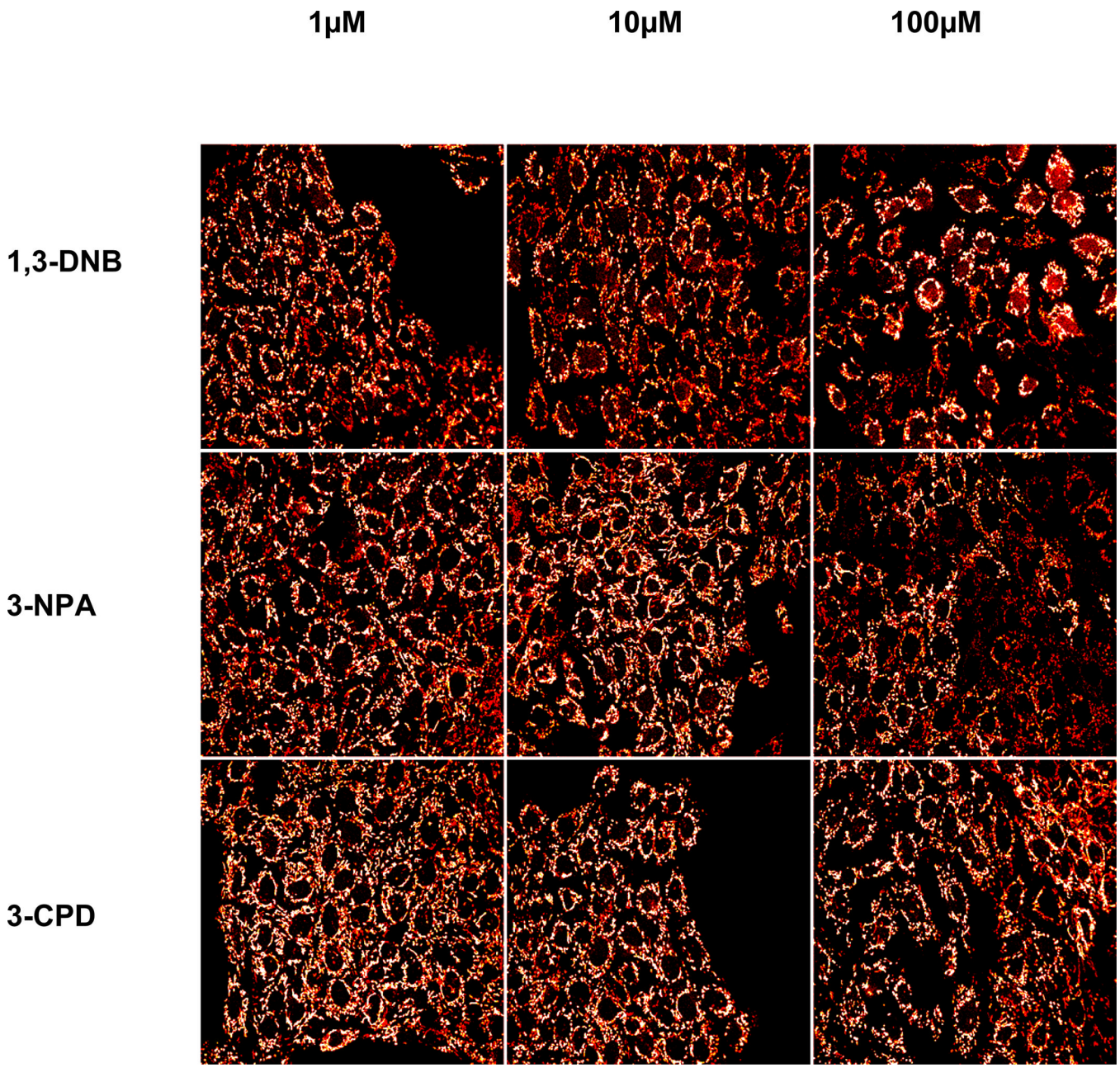

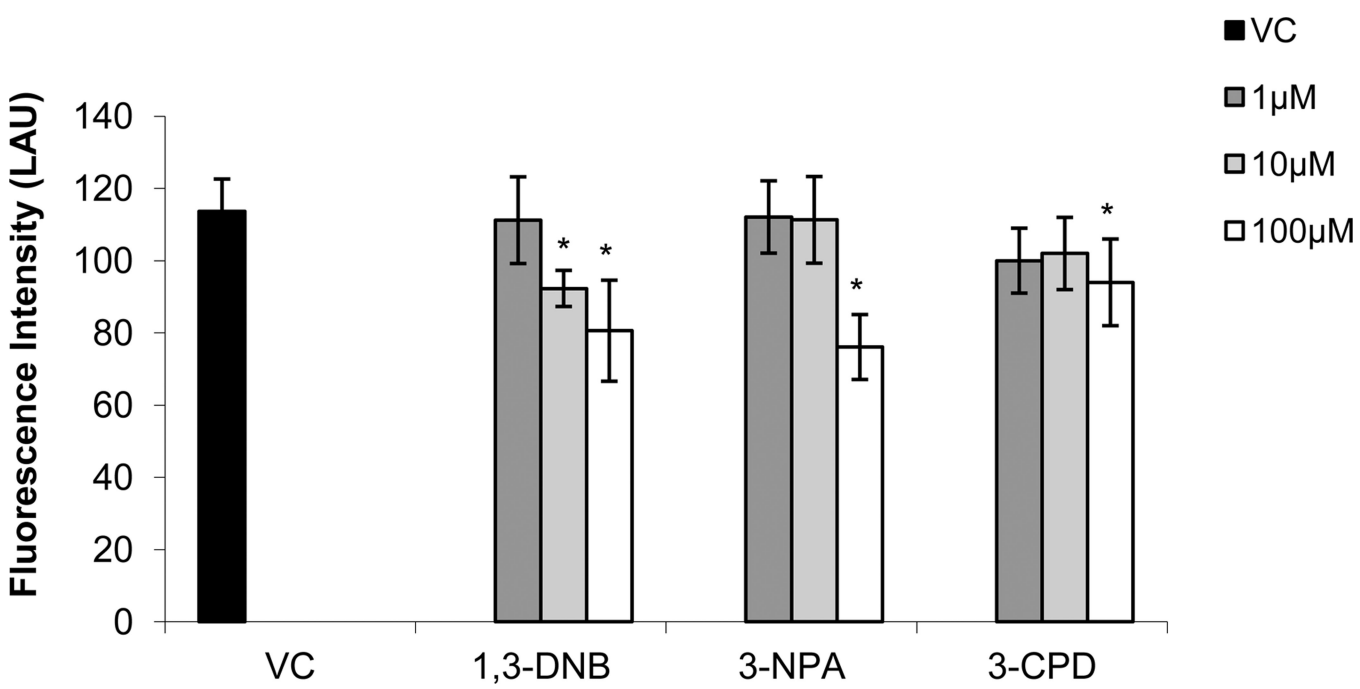

Figure 3.

Concentration-dependent loss of $\Delta\Psi_m$ in DI TNC1 cells measured over a 48 hr period using confocal microscopy. DI TNC1 cells were loaded with TMRM for 15 minutes after being pretreated with 600 μM deferoxamine and then exposed to either 1 μM, 10 μM, or 100 μM concentrations of 1,3-DNB, 3-NPA, or 3-CPD. Changes in TMRM fluorescence after a 48 hr exposure to each toxicant were measured and graphed as linear arbitrary units (LAU) in three independent experiments (8–10 cells per experiment). Values are expressed as mean ± SEM with statistical significance if $p < 0.05$ when compared to DMSO vehicle control (*).

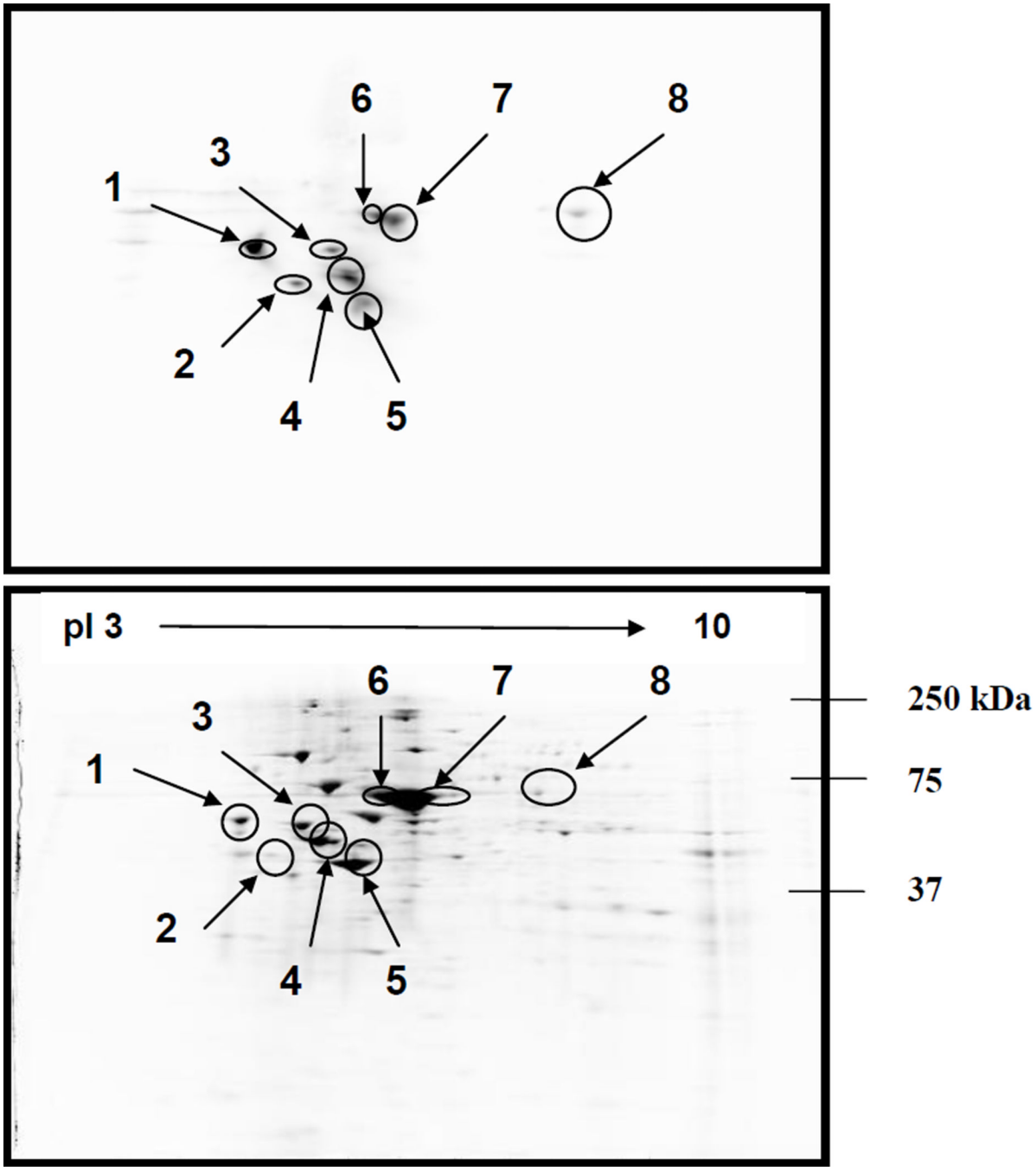

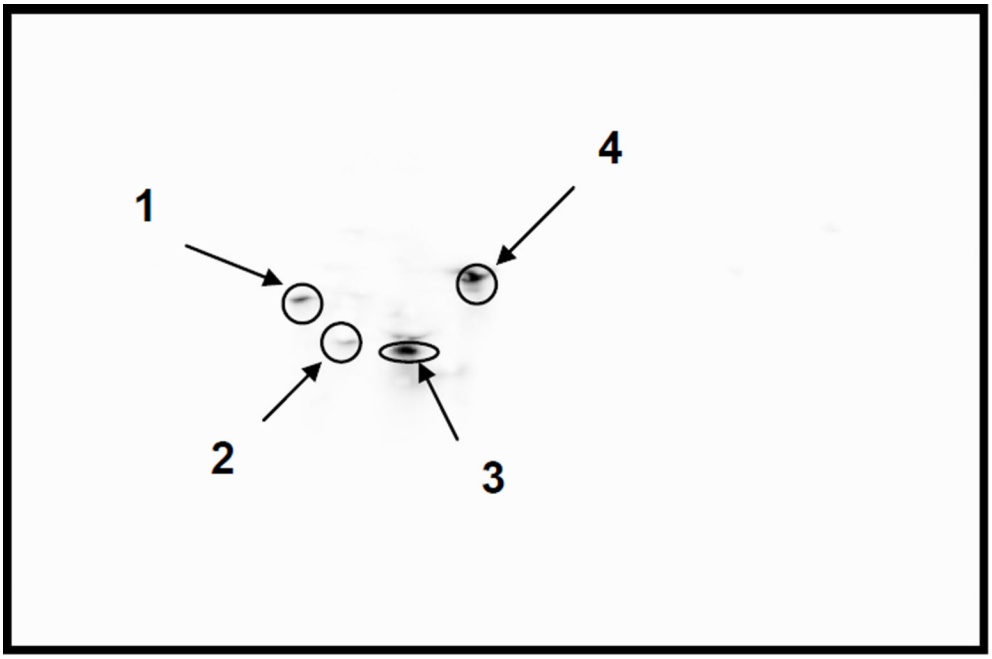

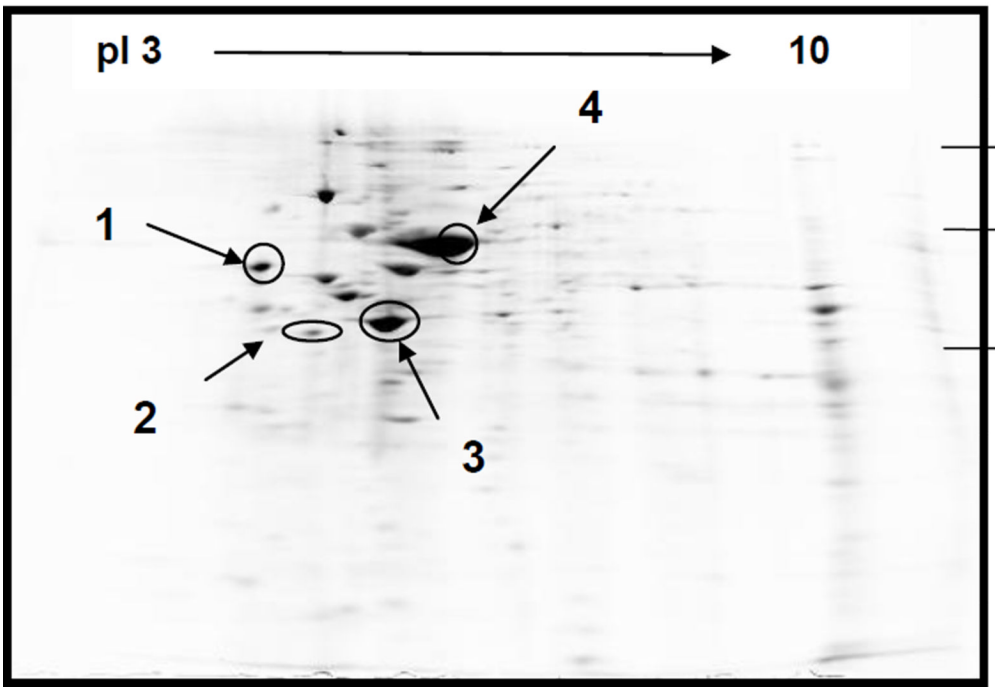

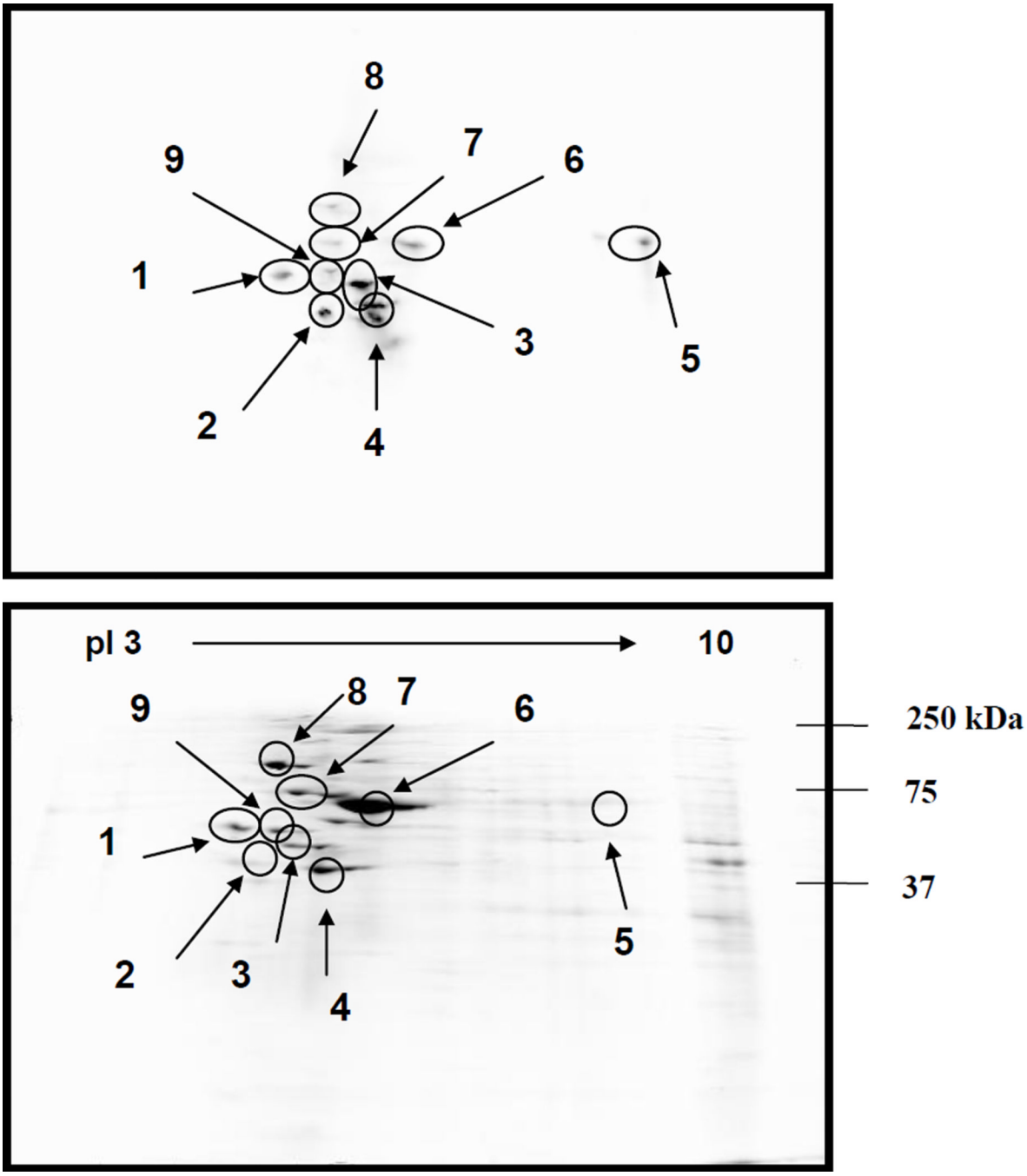

Table 1

Tandem mass spectrometric analysis of carbonylated proteins isolated from DI TNC1 cells after exposure to 100 μM 1,3-DNB for 48 hours. The Oxyblot image (top) is matched with its corresponding 2D gel (bottom).

Spot Label and Protein Name	Accession Number	Unused ProtScore	Confidence (%)	Number of Peptide Sequences Identified	Best Peptide Sequence	Total Ion Score
1. Calreticulin precursor	IPI00191728.1	16	99	12	CKDDEFTHLYTLIVRPDNTYEVK	177
2. LOC361571 38 kDa; predicted reticulocalbin 3 EF-hand calcium binding domain	IPI00782427.1; IPI00207050.5	5.7	99	5	EFDQLTPEESQAR	56
3. Protein disulfide-isomerase precursor	IPI00198887.1	24	99	12	HNQLPLVIEFTEQTAPK	208
4. F1 ATP synthase beta-subunit, mitocondrial precursor	IPI00551812.1	18.24	99	14	LVLEVAQHLGESTVR	223
5. Actin, cytoplasmic 2; actin, cytoplasmic 1	IPI00767505.1; IPI00765011.1; IPI00764461.1; IPI00189819.1	18	99	12	VAPEEHPVLLTEAPLNPK	219
6. Serum albumin precursor	IPI00191737.6	3.4	99	2	LGEYGFQNAVLVR	29
7. Serum albumin precursor	IPI00191737.6	4	99	2	LGEYGFQNAVLVR	34
8. Low abundance peak consistent with albumin						

Table 2

Tandem mass spectrometric analysis of carbonylated proteins isolated from DI TNC1 cells after exposure to 100 μM 3-CPD for 48 hours. The Oxyblot (top) is matched with its corresponding 2D gel (bottom).

Spot Label and Protein Name	Accession Number	Unused ProtScore	Confidence (%)	Number of Peptide Sequences Identified	Best Peptide Sequence	Total Ion Score
1. Calreticulin precursor	IPI00191728.1	17.4	99	13	CKDDEFTHLYTLIVRPDNTYEVK	191
2. LOC361571 38 kDa; predicted reticulocalbin 3 EF-hand calcium binding domain	IPI00782427.1; IPI00207050.5	6.27	99	9	EFDQLTPEESQAR	90
3. Actin, cytoplasmic 2; actin, cytoplasmic 1	IPI00767505.1; IPI00765011.1; IPI00764461.1; IPI00189819.1	18	99	11	VAPEEHPVLLTEAPLNPK	195
4. Serum albumin precursor	IPI00191737.6	2.04	99	2	LGEYGFQNAVLVR	28

Table 3

Tandem mass spectrometric analysis of carbonylated proteins isolated from DI TNC1 after exposure to 100 μM 3-NPA for 48 hours. The Oxyblot (top) is matched with its corresponding 2D gel (bottom).

Spot Label and Protein Name	Accession Number	Unused ProtScore	Confidence (%)	Number of Peptide Sequences Identified	Best Peptide Sequence	Total Ion Score
1. Calreticulin precursor	IPI00191728.1	15.28	99	12	GQTLVVQFTVK	133
2. 40S ribosomal protein SA	IPI00215107	5.15	99	3	FTPGTFTNQIQAAFR	44
3. F1 ATP synthase beta-subunit, mitocondrial precursor	IPI00551812.1	14.3	99	12	LVLEVAQHLGESTVR	181
4. Actin, cytoplasmic 2; actin, cytoplasmic 1	IPI00767505.1; IPI00765011.1; IPI00764461.1; IPI00189819.1	16	99	10	VAPEEHPVLLTEAPLNPK	163
5. D19Bwg1357e protein; pumilio domain-containing protein KIAA0020 homolog	IPI00767194.1; IPI00563669.1; IPI00371694.3	1.22	94	1	RRELLESISPAL	13
6. Low abundance peak consistent with albumin						
7. Hspa5, Grp78 kDa glucose-regulated protein precursor	IPI00206624.1	18.75	99	12	DNHLLGTFDLTGIPPAPR	182
8. Tumor rejection antigen gp96; predicted 93 kDa protein	IPI00734561.1; IPI00365985.4	20	99	12	FQSSHHSTDITSLDQYVER	168
9. Protein disulfide-isomerase, precursor	IPI00198887.1	21.9	99	12	VDATEESDLAQQYGVR	197